Proc. 2001 Australian Conference on Robotics and Automation
Sydney, 14-15 November 2001

Dragline Bucket and Rigging Dynamics

Dr Peter Ridley and Rindert Algra
School of Mechanical Engineering,
Queensland University of Technology,
GPO Box 2434, Brisbane 4001, Australia,
p.ridley@qut.edu.au

Dr Peter Corke
CSIRO Manufacturing Science and Technology,
QCAT PO Box 883, Kenmore 4069,
Australia,
pic@cat.csiro.au

Abstract

This paper is a continuation of work originally undertaken by the authors which predicts the static pose of a 1:20 scale dragline bucket and rigging throughout its workspace. Based on the results of this prior work, a two degree of freedom pendulum model is used to describe the dynamic response of the bucket to a small velocity inputs of the drag-rope. Linear differential equations, valid for small perturbations about the equilibrium pose, are used to predict the change in drag-rope tension and angular velocity of the bucket. Experimental frequency responses of these force and velocity transfer functions are used to confirm the mathematical model.

1 Introduction

1.1 Dragline Automation

Draglines (Figure 1 and 2) are the largest pick and place robots in existence. Using booms of 100 metres length, they strip over-burden from open cut coal mines 120 tonnes at a time. Incentive to automate the dragline comes from the possibility of increased productivity over manual operation. An additional benefit which may also flow, is the reduction in maintenance costs due to control of peak overloads. Such overloads arise from poor manual operation of the machine, often due to driver fatigue over long shifts. Considerable success has already been achieved on full-size machines, [Winstanely et al 1997], in automating the swing axis. This work has focused on the minimisation of cycle time by controlling the out of plane pendulum swing of the bucket as the dragline slews from dig to dump points. Under manual operation, motion control of the bucket in the plane of the boom is obtained, through simultaneous control of the hoist and drag-rope winch speeds. The hoist axis primarily provides lift, whilst the drag rope is used to regulate the bucket angle throughout the hoisting operation. Automatic control of the drag and hoist axes has not been achieved on full-size machines. This is the ultimate goal of the current research.

2 Static Pose

Dragline bucket and rigging form an under actuated mechanism which finds an equilibrium pose at a position of minimum potential energy. Calculation of the static pose of this mechanism is discussed in detail by the authors [Ridley and Corke 2000] who experimentally verified their results on a 1:20 scale model. For a particular load configuration, the workspace can be described as a set of contours of equal bucket carry angle (γ) as shown in Figure 1. These contours are not fixed. As the location of centre of gravity changes so do locations of the carry angle contours. Figure 4 shows a free-body diagram, containing the bucket and rigging of known mass m, at equilibrium. The following features can be calculated for the 1:20 scale model along a given carry angle contour.

- positions of the intersection point I, hitch-point H, drag-point D and centre of gravity C,
- hoist-rope angle λ, drag-rope angle δ tension T_d,
- lengths l_1,l_2, l_3 and angles $\overline{\theta}_1$, $\overline{\theta}_2$ and $\overline{\theta}_3$,
- mass moment of inertia J_C of the system, about the centre of gravity C,
- the distance c^* of the centre of gravity above the intersection point I.

3 Bucket Acceleration Analysis

Given that the static pose of the bucket and rigging may be calculated at any location within the workspace, it is now possible to calculate the initial acceleration of the bucket subjected to a small additional drag-rope load t_d above the static load T_d. This applied force, shown in Figure 4, induces an additional load t_h in the hoist rope and causes an angular acceleration of the body is $\ddot{\gamma}$.

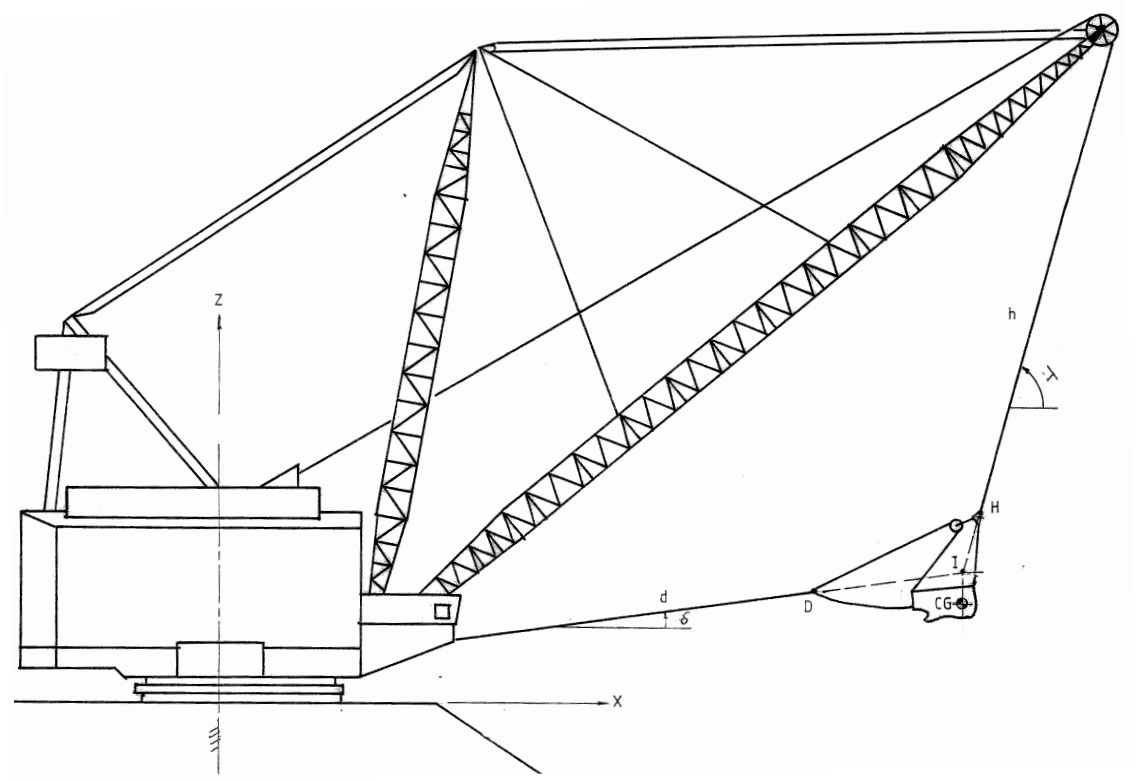

Figure 1: Dragline

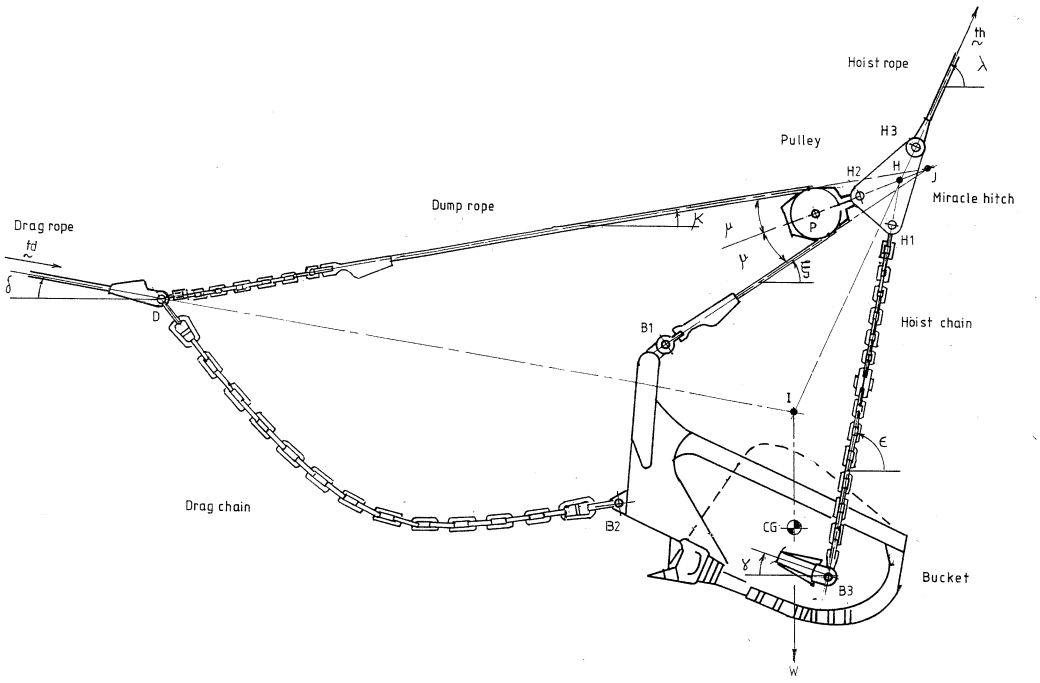

Figure 2: Bucket rigging

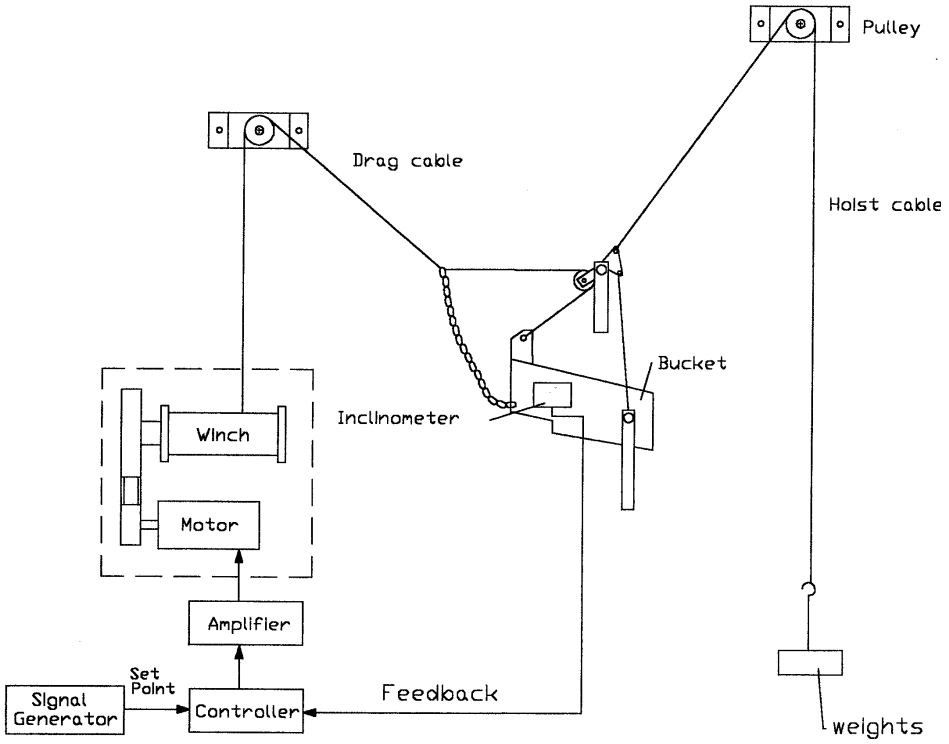

Figure 3: Experimental apparatus

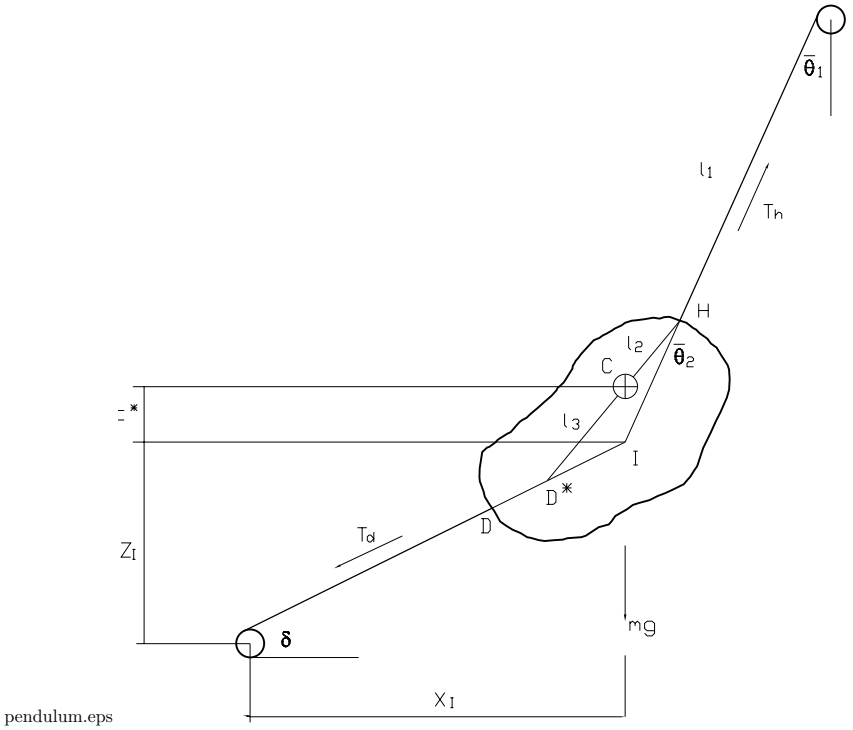

pendulum.eps

Figure 4: Pendulum model

Applying Newton's second law of motion in the x- and z-directions:

$$-t_d cos\delta + t_h cos\lambda = m\ddot{x}_C \quad (1)$$

$$t_h sin\lambda - t_d sin\delta = m\ddot{z}_C \quad (2)$$

The moment acting about the system centre of gravity, C ,equals the rate of change of angular momentum of the system about C, $\Sigma M_C = \dot{H}_C$. Since the only significant mass in the system is the bucket and load, this relationship may be simplified $\Sigma M_C = J_C\ddot{\gamma}$.

$$-t_h c^* cos\lambda + t_d c^* cos\delta = J_C\ddot{\gamma} \quad (3)$$

Assuming that the normal component of acceleration at point H is negligible.

$$\ddot{x}_C cos\lambda + \ddot{\gamma}c^* cos\lambda + \ddot{z}_C sin\lambda = 0. \quad (4)$$

Once the unwanted variables are eliminated between the equations (1)-(4), it can be shown that:

$$\frac{\ddot{\gamma}}{t_d} = c^* \left[\frac{cos\delta - cos\lambda cos(\delta - \lambda)}{J_C - mc^{*2} cos\lambda}\right] \quad (5)$$

If this ratio is negative, an initial downward tilting angular acceleration occurs when tension is applied to the drag rope. However from the carry angle contours it is also apparent that hauling on the drag rope will eventually cause the body to tilt upwards. Dynamic response, in which the motion starts in the opposite direction to that which it finally moves, is associated with non-minimum phase behavior. The bracketed expression in equation 5 is a positive quantity. (NB: $80^o<\lambda<90^o$ and $-50^o<\delta<25^o$). Hence it may be concluded that non-minimum phase behavior occurs when the centre of gravity C lies below the point of intersection of drag and hoist rope axes I.

4 Dynamic model

The dynamic model considered here (Figure 4) describes the perturbation of the bucket from its static equilibrium, by a drag-rope velocity v. This induces a small drag-rope force t_d and hoist rope force t_h. Small angular displacements θ_1 and θ_2 result. It is assumed that drag-rope is sufficiently long to ensure that angle δ remains essentially constant.

An overall transfer function, $G(s)$, is used to relate the drag rope velocity v to angular velocity $\dot{\gamma}$ of the bucket. $G(s)$ is subdivided into two transfer functions $G_1(s)$ and $G_2(s)$ as shown in Figure 5.

- $\frac{f(s)}{v(s)} = G_1(s)$ expresses the relationship between the input drag rope velocity v and the forces f created in the drag rope as a result of the motion of the bucket,
- $\frac{\dot{\gamma}(s)}{t_d(s)} = G_2(s)$ expresses the relationship between the out of balance drag rope force t_d and the angular velocity $\dot{\gamma}$ of the bucket.
- external forces f_e acting on the bucket are shown entering between $G_1(s)$ and $G_2(s)$. $t_d = f + f_e$.

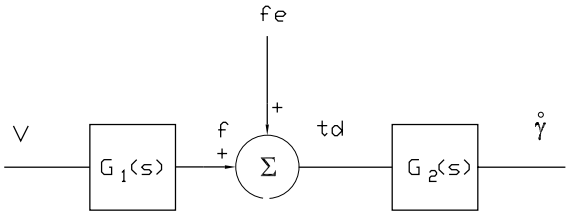

Figure 5: Block diagram

4.1 Rigid Body Model

If the assumption is made that the rigging remains rigid, a two degree of freedom model , shown in Figure 4, may be derived. The angular velocity of the bucket $\dot{\gamma} = \dot{\theta}_{12}$. A pair of simultaneous linear differential equations describe the motion about the equilibrium pose. Coefficients (a_i,b_i, etc) are summarised in the Appendix of this paper.

$$a_1\ddot{\theta}_1 + a_2\dot{\theta}_1 + a_3\theta_1 + a_4\ddot{\theta}_2 = a_5 t_d \quad (6)$$

$$b_1\ddot{\theta}_1 + b_2\dot{\theta}_1 + b_3\theta_1 + b_4\ddot{\theta}_2 + b_5\dot{\theta}_1 + b_6\theta_1 = b_7 t_d \quad (7)$$

The transfer functions derived from these differential equations relating the displacements to the applied force on the drag-rope are:

$$\frac{\dot{\theta}_1(s)}{t_d(s)} = \frac{s(e_1 s^2 + e_2 s + e_3)}{d_1 s^4 + d_2 s^3 + d_3 s^2 + d_4 s + d_5} \quad (8)$$

$$\frac{\dot{\theta}_2(s)}{t_d(s)} = \frac{s(f_1 s^2 + f_2 s + f_3)}{d_1 s^4 + d_2 s^3 + d_3 s^2 + d_4 s + d_5} \quad (9)$$

$$G_2(s) = \frac{\dot{\theta}_{12}(s)}{t_d(s)} = \frac{s(g_1 s^2 + g_2 s + g_3)}{d_1 s^4 + d_2 s^3 + d_3 s^2 + d_4 s + d_5} \quad (10)$$

The transfer function between the input velocity v of the drag-rope and the drag-rope tension t_d may be evaluated from equations (8) and (9).

$$\frac{v(s)}{t_d(s)} = l_1\frac{\dot{\theta}_1(s)}{t_d(s)}cos(\overline{\theta}_1+\delta)+l_{23}\frac{\dot{\theta}_{12}(s)}{t_d(s)}cos(\overline{\theta}_{12}+\delta) \quad (11)$$

which may be expressed,

$$G_1(s) = \frac{t_d(s)}{v(s)} = \frac{d_1 s^4 + d_2 s^3 + d_3 s^2 + d_4 s + d_5}{s(h_1 s^2 + h_2 s + h_3)}. \quad (12)$$

Roots of the fourth order characteristic equation

$$d_1 s^4 + d_2 s^3 + d_3 s^2 + d_4 s + d_5 = 0 \quad (13)$$

identify the natural two frequencies of the system, which are plotted, for the 1:20 scale model in Figure 6.

$$G(s) = G_1(s)G_2(s) = \frac{g_1 s^2 + g_2 s + g_3}{h_1 s^2 + h_2 s + h_3}. \quad (14)$$

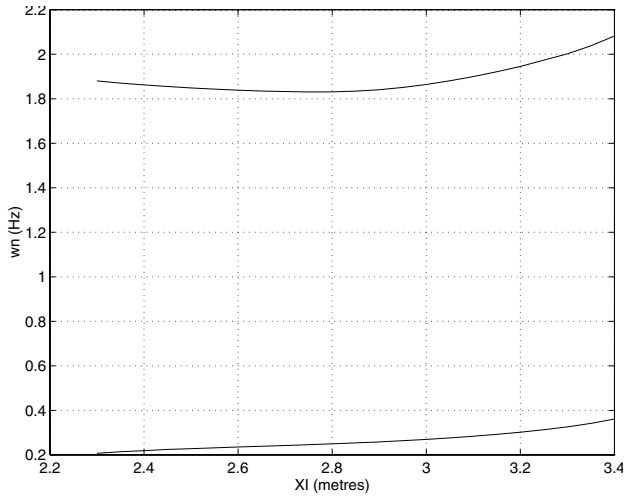

Figure 6: Rigid body natural frequencies.

5 Non-minimum phase systems

Systems whose poles lie in the left-hand plane but whose zeroes lie in the right hand-plane are stable, yet do not exhibit minimum phase characteristics. The rigid body assumption leads us to believe that system may be modeled with two poles and two zeroes.

$$G(s) = K\frac{s^2 + 2\xi_z\omega_z + \omega_z^2}{s^2 + 2\xi_p\omega_p + \omega_p^2}. \qquad (15)$$

When $\xi_z > 0$ the system exhibits minimum phase characteristic, shown by the solid line in the phase plot of Figure 7. Non-minimum phase behavior, shown by a broken line, occurs when $\xi_z < 0$.

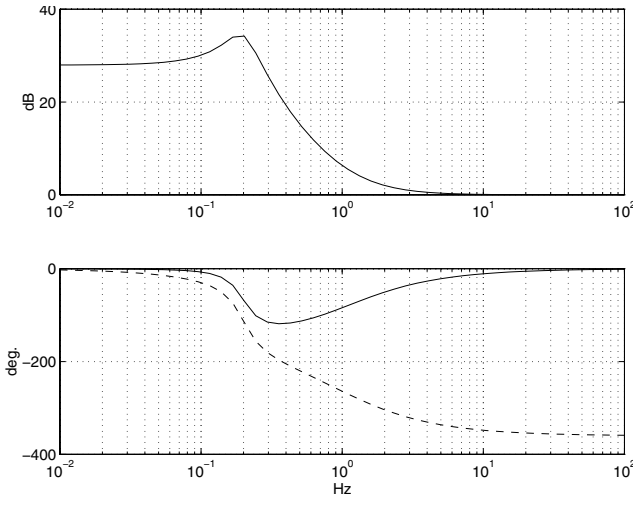

Figure 7: Frequency response plot: $\omega_z = 1.0Hz, \xi_z = \overset{+}{-} 1.0$ $\omega_p = 0.2Hz, \xi_p = 0.25$

6 Experimental results

6.1 Method

Layout of experimental apparatus is shown in Figure 3. The 1:20 scale bucket was equipped with a motor and winch on the drag-rope. Frequency responses are measured using a dual channel spectrum analyser for twelve different bucket locations in the workspace along a single bucket carry angle contour.

Implementation of a weak position feedback loop , using an inclinometer in the feedback path, ensures that the pose of the bucket does not drift throughout each trial. Investigation of the bucket/rigging dynamics was carried out by applying a swept sine voltage to the controller input.

6.2 Frequency responses

Force response

Typical responses, between the input voltage to the amplifier V and the voltage V_f from the drag-rope force transducer. $G_1(s) = \frac{V_f}{V}$ are plotted in Figure 8 at the middle of the workspace. These show two distinct anti-resonances, as predicted by the model, at the pendulum natural frequencies.

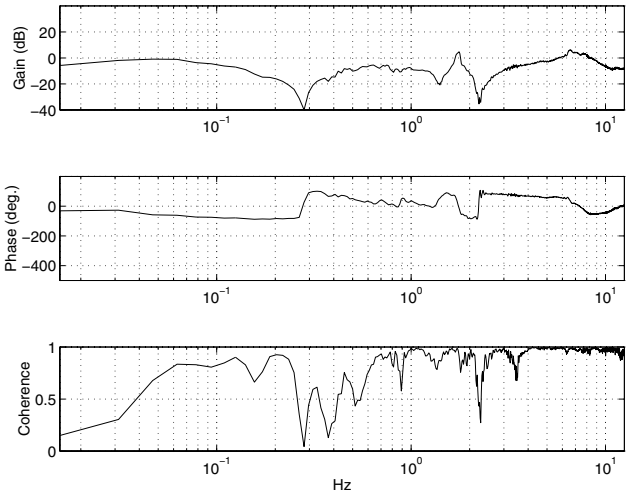

Figure 8: Force response at location 6 $\frac{V_f}{V}$

Velocity response

A typical velocity responses $G(s) = \frac{V_\dot{y}}{V}$ is plotted in Figure 9 at middle of the workspace.

The dashed lines on these graphs are the frequency responses of the best fit two-pole/two zero model described in equation 15. The poles and zeroes of this fitted model, at the twelve locations along the carry angle contour, are plotted in Figure 10. Presence of zeroes in the right-hand plane confirms the non-minimum phase characteristic of the transfer function.

7 Conclusions

This paper has shown that the lower order dynamics of the dragline bucket may be described by a two degree of freedom rigid body model of the bucket and rigging. It is anticipated that this model will be useful in scaling the experimental results obtained from the 1:20 scale model up to full-size machines.

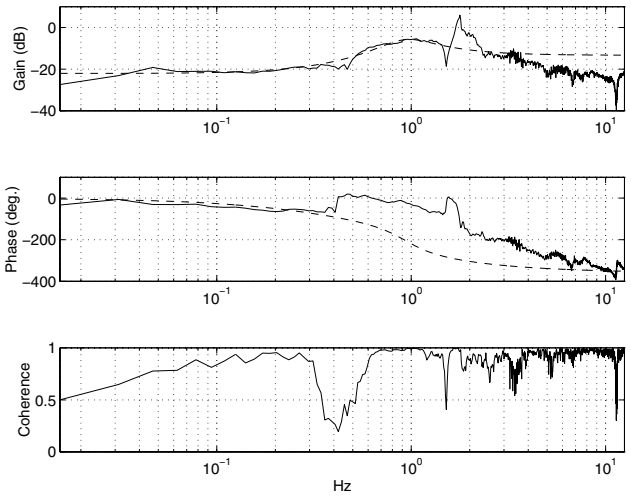

Figure 9: Velocity response at location 6 $\frac{V_7}{V}$

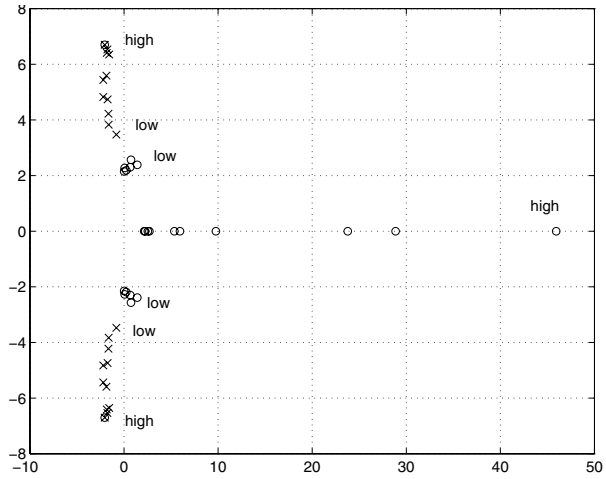

Figure 10: Locus of zeroes and poles throughout the workspace

The model successfully explains the observed non-minimum phase behavior of the system dynamics. Non-minimum phase behavior is undesirable in plant where feedback control strategies are to be implemented. High plant gain and rapidly falling phase, associated with such systems, inevitably leads to low gain, low bandwidth loop controllers, which are needed to establish a stable closed loop response.

The model shows that the system poles, in $G_2(s)$ associated with the natural frequencies of the pendulum are canceled by the anti-resonances (zeroes) in the force response $G_1(s)$. Hence the natural pendulum modes uncontrollable, resulting in poor rejection of force disturbances in the closed loop system. This explains the difficulties, described by the authors [Ridley and Corke 2001], in achieving satisfactory automatic control of bucket carry angle.

Cancellation will not occur if the winch motor is driven by a current amplifier. In this case the bucket would be actuated by a drag-rope force, not a velocity. This is a design change which will be implemented in future experiments.

Acknowledgements

The authors wish to acknowledge the assistance given to the project by engineering undergraduate students Fong Kah Yung (Queensland University of Technology) and Miso Montonen (Helsinki University of Technology).

References

[Winstanley et al. 1997], Winstanley G.J., Corke P.I., Roberts J.M., Dragline swing automation. *IEEE International International Conference on Robotics and Automation* 1997, pp1827-1832.

[Ridley and Corke 2000], Ridley P.R., Corke P.I., Calculation of dragline bucket pose under gravity loading. *Mechanism and Machine Theory*, 35 (2000), pp1431-1444

[Ridley and Corke 2001] Ridley P.R., Corke P.I., Dragline automation.*Proceedings of IEEE International Conference on Robotics and Automation*, May 2001, Seoul, pp3742 - 3747

Appendix

Differential equation coefficients

$a_1 = m(l_1 + l_2 cos\theta_2)$
$a_2 = B_1$
$a_3 = \frac{mgcos\delta}{cos(\theta_1+\delta)}$
$a_4 = ml_2 cos\theta_2$
$a_5 = cos(\theta_1 + \delta)$

$b_1 = J_C sin\theta_1 - ml_2{}^2 sin\theta_2 cos\theta_{12} - ml_1 l_2 sin\theta_2 cos\theta_1$
$b_2 = -B_1 l_2 sin\theta_{12}$
$b_3 = \frac{-mg}{cos(\theta_1+\delta)}(l_2 cos\delta cos\theta_1 sin\theta_2 - l_3 sin^2\theta_1 sin(\theta_{12} + \delta))$
$b_4 = J_C sin\theta_1 - ml_2^2 sin\theta_2 cos\theta_{12}$
$b_5 = B_2 sin\theta_1$
$b_6 = \frac{mg}{cos(\theta_1+\delta);}(l_2 cos\delta sin\theta_1 cos\theta_2 + l_3 sin^2\theta_1 sin(\theta_{12} + \delta))$
$b_7 = -l_2 sin\theta_2 cos\delta + l_3 cos(\theta_{12} + \delta) sin\theta_1$

$e_1 = a_5 b_4 - a_4 b_7$
$e_2 = a_5 b_5$
$e_3 = a_5 b_6$

$f_1 = a_1 b_7 - a_5 b_1$
$f_2 = a_2 b_7 - a_5 b_2$
$f_3 = a_3 b_7 - a_5 b_3$

$g_1 = e_1 + f_1$
$g_2 = e_2 + f_2$
$g_3 = e_3 + f_3$

$h_1 = l_1 cos(\theta_1 + \delta)e_1 + l_{23} cos(\theta_{12} + \delta)(e_1 + f_1)$
$h_2 = l_1 cos(\theta_1 + \delta)e_2 + l_{23} cos(\theta_{12} + \delta)(e_2 + f_2)$
$h_3 = l_1 cos(\theta_1 + \delta)e_3 + l_{23} cos(\theta_{12} + \delta)(e_3 + f_3)$
$d_1 = a_1 b_4 - a_4 b_1$
$d_2 = a_1 b_5 + a_2 b_4 - a_4 b_2$
$d_3 = a_1 b_6 + a_2 b_5 + a_3 b_4 - a_4 b_3$
$d_4 = a_2 b_6 + a_3 b_5$
$d_5 = a_3 b_6$